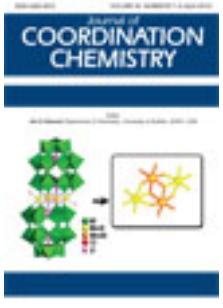

Journal of Coordination Chemistry
Publication details, including instructions for authors and subscription information:
http://www.tandfonline.com/loi/gcoo20

Synthesis, structure, and luminescence of rhenium(I) complexes with substituted bipyridines

Hong Xia [a], Xiaoming Liu [a b], Qiaolin Wu [b], Yuwei Zhang [b], Wei Gao [b] & Ying Mu [b]

[a] State Key Laboratory on Integrated Optoelectronics, College of Electronic Science and Engineering, Jilin University, Changchun 130012, People's Republic of China

[b] State Key Laboratory of Supramolecular Structure and Materials, School of Chemistry, Jilin University, Changchun 130012, People's Republic of China

Published online: 20 Mar 2012.

To cite this article: Hong Xia, Xiaoming Liu, Qiaolin Wu, Yuwei Zhang, Wei Gao & Ying Mu (2012) Synthesis, structure, and luminescence of rhenium(I) complexes with substituted bipyridines, Journal of Coordination Chemistry, 65:7, 1266-1277, DOI: 10.1080/00958972.2012.671479

To link to this article: http://dx.doi.org/10.1080/00958972.2012.671479

Journal of Coordination Chemistry
Vol. 65, No. 7, 10 April 2012, 1266–1277

Synthesis, structure, and luminescence of rhenium(I) complexes with substituted bipyridines

HONG XIA†, XIAOMING LIU*†‡, QIAOLIN WU‡, YUWEI ZHANG‡, WEI GAO‡ and YING MU‡

†State Key Laboratory on Integrated Optoelectronics, College of Electronic Science and Engineering, Jilin University, Changchun 130012, People's Republic of China
‡State Key Laboratory of Supramolecular Structure and Materials, School of Chemistry, Jilin University, Changchun 130012, People's Republic of China

(*Received 13 October 2011; in final form 2 February 2012*)

Two new rhenium(I) complexes chelated by a substituted 2,2′-bipyridine with general formula $Re(CO)_3LCl$, where L = 6-(2″-methoxyphenyl)-2,2′-bipyridine (**L_1**) and 6-(4″-diphenylamino-phenyl)-2,2′-bipyridine (**L_2**), are synthesized and characterized by IR, NMR, and elemental analysis. Structure of **1** was determined by single-crystal X-ray crystallography, revealing that rhenium is six-coordinate octahedral. The electrochemical, photophysical, and thermal properties of the two rhenium(I) complexes were investigated. Electroluminescent devices were fabricated by doping **1** in polymer blend host of poly(vinylcarbazole) and 2-tert-butylphenyl-5-biphenyl-1,3,4-oxadiazole using simple solution spin-coating technique. The device exhibits a maximum current efficiency of 2.97 cd A^{-1} and peak brightness in excess of 2390 cd m^{-2}.

Keywords: Bipyridine; Rhenium complex; Phosphorescent; Electroluminescence

1. Introduction

Employment of heavy metal complexes as emitters in organic light-emitting diodes (OLEDs) has become important since the original works of Thompson *et al*. [1]. OLEDs based on phosphorescent materials show remarkable enhancement in their electroluminescent (EL) performance and exhibit higher internal quantum efficiency of up to 100% in principle. Iridium(III) [2], platinum(II) [3], and ruthenium(II) [4] complexes have been exploited in OLEDs. Recent research demonstrates that rhenium(I) complexes also serve as electrophosphorescent emitters for OLEDs with features of high room temperature phosphorescence quantum yield, relatively short excited state lifetime and photochemical stability [5–7]. Rhenium(I) complexes with different ligands have been reported and applied as emitters in OLEDs [5–8]. For example, Li *et al*. [5a] reported efficient devices based on (2,9-dimethyl-1,10-phenanthroline)$Re(CO)_3Cl$ doped into 4,4′-*N*,*N*′-dicarbazole-biphenyl (CBP) with a current efficiency of 7.15 cd A^{-1}. Recently, the group of Li and Chu [6b] reported more

*Corresponding author. Email: xm_liu@jlu.edu.cn

ISSN 0095-8972 print/ISSN 1029-0389 online
http://dx.doi.org/10.1080/00958972.2012.671479

efficient OLEDs based on (2,9-dimethyl-4,7diphenyl-1,10-phenanthroline)$Re(CO)_3Br$ with a maximum EL efficiency and luminance of 21.8 cd A^{-1} and 8315 cd m^{-2}, respectively. Utilizing the vacuum-deposition method, OLEDs based on rhenium(I) complexes show high efficiency and luminance. However, the sublimation process has critical drawbacks including considerable loss of the expensive materials during evaporation, complex manufacturing process, and high manufacturing costs. Therefore, solution processed OLEDs attract attention as potential candidates for large area flat panel displays, owing to their simple processing route and low manufacturing cost. Rhenium(I) complex-based devices made by a solution process are less reported and show relatively low efficiency and luminescence [9]. Hence, we hope to synthesize soluble rhenium(I) complexes and further fabricate efficient phosphorescent devices by the spin-casting solution process. We consider that the introduction of bulky group on the six-position of 2,2′-bipyridine can decrease molecular stacking of a rhenium complex and restrain triplet–triplet annihilation. Therefore, in this article, we report the syntheses, electrochemical, photophysical, and thermal properties, as well as EL behaviors of new rhenium(I) complexes with substituted 2,2′-bipyridine ligands.

2. Experimental

2.1. *General procedures*

All reactions were performed using standard Schlenk techniques in an atmosphere of high-purity nitrogen. Toluene was dried by refluxing over sodiumbenzophenone and distilled under nitrogen prior to use. Solvents used in luminescence and electrochemical studies were anhydrous and spectroscopic grade. Dimethylformamide (DMF), tetrahydrofuran (THF), dimethyl sulfoxide (DMSO), dichloromethane (CH_2Cl_2), tetrabutylammonium tetrafluoroborate (Bu_4NBF_4), poly(vinylcarbazole) (PVK), 2-tert-butylphenyl-5-biphenyl-1,3,4-oxadiazole (PBD), 1,3,5-tri(1-phenyl-1 H-benzo[d]imidazol-2-yl)phenyl (TPBI), poly(3,4-ethylenedioxythiophene) : poly(styrenesulfonate) (PEDOT : PSS), 2,2′-bipyridine, $Re(CO)_5Cl$, and ^{n}BuLi were purchased from Aldrich and used as received. NMR spectra were measured on a Varian Mercury-300 spectrometer. Fourier transform infrared spectroscopy (FT-IR) spectra were acquired using a Magna 560 FT-IR spectrophotometer. Elemental analyses were performed on a Perkin-Elmer 2400 analyzer. UV-Vis absorption spectra were recorded on a UV-3100 spectrophotometer (Shimadzu) and fluorescence measurements were carried out on an RF-5301PC spectrophotometer (Shimadzu). Time-resolved fluorescence measurements were performed by the time-correlated single photon counting (TCSPC) system under right-angle sample geometry. A 379 nm picosecond diode laser (Edinburgh Instruments EPL375, repetition rate 20 MHz) was used to excite the sample. The emission was detected by a photomultiplier tube (Hamamatsu H5783p) and a TCSPC board (Becker & Hickel SPC-130). The instrument response function (IRF) is 220 ps. Thermogravimetric analysis (TGA) was performed using a Perkin-Elmer thermal analyzer in air. The samples were dried under vacuum at 60°C before being heated to 600°C at a heating rate of 10°C min^{-1}. Electrochemical measurements were performed with a BAS 100 W bioanalytical system using a platinum disc ($\varphi = 3$ mm) as the working

electrode, a platinum wire as the auxiliary electrode, and a porous glass wick Ag/Ag^+ as the reference electrode with ferrocenium–ferrocene (Fc^+/Fc) as the internal standard.

2.2. *Preparation*

2.2.1. 6-(2″-methoxyphenyl)-2,2′-bipyridinerhenium chlorotricarbonyl (1). $Re(CO)_5Cl$ (100 mg, 0.27 mmol) and $\mathbf{L_1}$ (73.4 mg, 0.28 mmol) were refluxed in 20 mL of toluene for 8 h. After the mixture cooled to room temperature, the solvent was removed in a water bath under reduced pressure. The resulting yellow solid was purified by silica gel column chromatography with ethyl acetate and CH_2Cl_2. Yield: 0.123 g (80%). ^{1}H NMR (300 MHz, DMSO-d_6, 293 K): δ 3.76 (s, 3 H, OCH_3), 7.10–7.27 (m, 3 H), 7.54 (t, 1 H), 7.66 (d, 1 H), 7.73 (t, 1 H), 8.32 (m, 2 H), 8.77 (m, 2 H), 9.02 (d, 1 H) ppm. Anal. Calcd for $C_{20}H_{14}ClN_2O_4Re$ (568.00): C, 42.29; H, 2.48; N, 4.93. Found: C, 42.52; H, 2.56; N, 4.85. IR (KBr): ν 1880, 1910, 2018 cm^{-1}.

2.2.2. 6-(4″-diphenylaminophenyl)-2,2′-bipyridinenerhenium chlorotricarbonyl (2). The procedure for the synthesis of **2** is similar to that for **1**, except that ligand $\mathbf{L_1}$ is replaced with $\mathbf{L_2}$. Yield: 0.123 g (85%). ^{1}H NMR (300 MHz, DMSO-d_6, 293 K): δ 7.10–7.14 (m, 2 H), 7.19 (d, 5 H), 7.44 (t, 5 H), 7.53–7.58 (m, 2 H), 7.82 (t, 1 H), 7.88 (d, 1 H), 8.38–8.42 (m, 2 H), 8.79 (d, 1 H), 8.83 (d, 1 H), 9.11 (d, 1 H) ppm. Anal. Calcd for $C_{31}H_{21}ClN_3O_3Re$ (705.18): C, 52.80; H, 3.00; N, 5.96. Found: C, 52.94; H, 2.86; N, 5.85. IR (KBr): ν 1870, 1922, 2024 cm^{-1}.

2.3. *X-ray crystallography*

Single crystals of **1** suitable for X-ray structural analysis were obtained from CH_2Cl_2. Diffraction data were collected at 293 K on a Rigaku R-AXIS RAPID IP diffractometer equipped with graphite-monochromated Mo-Kα radiation ($\lambda = 0.71073$ Å). Details of the crystal data, data collections, and structure refinements are summarized in table 1. The structure was solved by direct methods [10] and refined by full-matrix least-squares on F^2. All non-hydrogen atoms were refined anisotropically and the hydrogen atoms were included in idealized positions. All calculations were performed using the SHELXTL [11] crystallographic software package.

3. Results and discussion

3.1. *Synthesis and characterization of compounds*

The ligands $\mathbf{L_1}$ and $\mathbf{L_2}$ were prepared according to a known procedure [12]. Both were characterized by ^{1}H NMR spectroscopy along with elemental analyses. Reaction of $Re(CO)_5Cl$ with one equivalent of $\mathbf{L_1}$ or $\mathbf{L_2}$ in toluene at reflux afforded the corresponding complexes **1** and **2** in high yields (>80%) as yellow solids (figure 1). Two complexes were characterized by ^{1}H NMR spectroscopy, FT-IR, and satisfactory analytic results were obtained. The ^{1}H NMR spectra of **1** and **2** show that resonances of

Table 1. Crystal data and structure refinement details for **1**.

Empirical formula	$C_{20}H_{14}ClN_2O_4Re$
Molecular mass	567.98
Temperature (K)	293(2)
Wavelength (Å)	0.71073
Crystal system	Monoclinic
Space group	$P2(1)/c$
Unit cell dimensions (Å, °)	
a	13.560(3)
b	10.609(2)
c	13.914(3)
α	90
β	92.71(3)
γ	90
Volume (Å^3), Z	1999.5(7), 4
Calculated density (g cm^{-3})	1.887
$F(000)$	1088
Crystal size (mm^3)	$0.24 \times 0.16 \times 0.13$
θ range for data collection (°)	3.01–27.48
Limiting indices	$-17 \le h \le 17$; $-13 \le k \le 13$; $-18 \le l \le 16$
Data/restraints/parameters	4572/0/254
Goodness-of-fit on F^2	1.017
Final R indices [$I > 2\sigma(I)$]	$F_1{}^a = 0.0332$, $wF_1{}^b = 0.0722$
R indices (all data)	$F_1{}^a = 0.0434$, $wF_1{}^b = 0.0773$

$^aR_1 = \sum||F_o| - |F_c||/\sum|F_o|$; $^bwR_2 = [\sum[w(F_o^2 - F_c^2)^2]/\sum[w(F_o^2)^2]]^{1/2}$.

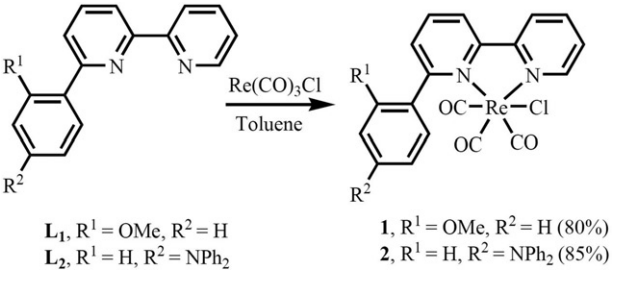

Figure 1. Synthetic procedure of rhenium complexes.

the protons on pyridine rings shift to low field compared to the corresponding signals in their free ligands, indicating formation of the coordination bonds between the ligand and rhenium(I) [13]. FT-IR spectra of both complexes show three stretching bands from 1869 to 2021 cm^{-1}, consistent with three carbonyl groups at the $Re(CO)_3$ metal fragment. Complex **1** is moderately soluble in DMSO, CH_2Cl_2, DMF, and THF, but insoluble in saturated hydrocarbons. Compared with **1**, **2** has less solubility in organic solvents.

3.2. *Structure of 1*

The molecular structure of **1** was determined by X-ray crystallographic analysis. Crystals of **1** suitable for X-ray crystal structure determination were grown from

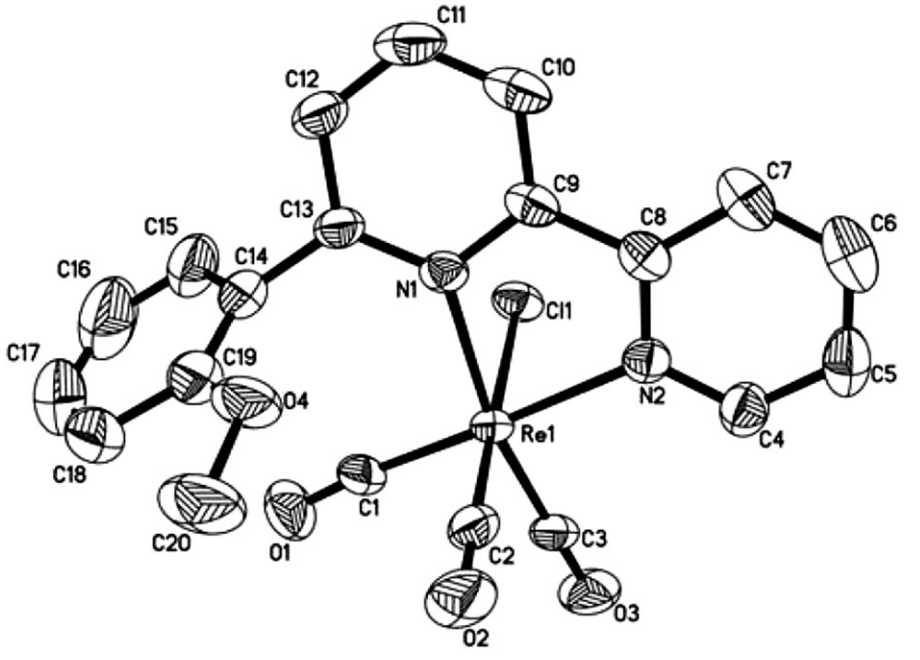

Figure 2. ORTEP drawing of **1** with displacement ellipsoids at the 30% probability level. Hydrogen atoms have been omitted for clarity.

Table 2. Selected bond lengths (Å) and angles (°) for **1**.

Re(1)–C(1)	1.900(6)	C(3)–Re(1)–N(2)	95.84(19)
Re(1)–C(2)	1.874(5)	C(1)–Re(1)–N(2)	177.61(18)
Re(1)–C(3)	1.888(5)	C(2)–Re(1)–N(1)	96.8(2)
Re(1)–N(1)	2.210(4)	C(3)–Re(1)–N(1)	168.69(17)
Re(1)–N(2)	2.164(4)	C(1)–Re(1)–N(1)	103.04(19)
O(1)–C(1)	1.147(6)	N(2)–Re(1)–N(1)	74.91(15)
O(2)–C(2)	1.166(6)	C(2)–Re(1)–Cl(1)	177.81(19)
O(3)–C(3)	1.151(6)	C(1)–Re(1)–Cl(1)	93.78(17)
C(2)–Re(1)–C(3)	90.1(2)	N(1)–Re(1)–Cl(1)	81.76(10)
C(2)–Re(1)–C(1)	88.1(2)	N(2)–Re(1)–Cl(1)	84.74(11)
C(3)–Re(1)–C(1)	86.1(2)	C(3)–Re(1)–Cl(1)	91.05(15)

CH_2Cl_2 at room temperature. The ORTEP drawing of the molecular structure of **1** is shown in figure 2. Selected bond lengths and angles for the complex are given in table 2. The X-ray analysis reveals that **1** adopts distorted octahedral geometry with the metal center chelated by $\mathbf{L_1}$ *via* two nitrogen atoms and the three carbonyls are facial. The distances of C(1), C(2), and C(3) to Re(1) are 1.900(6), 1.874(5), and 1.888(5) Å, respectively. These values are consistent with bond lengths found in other distorted octahedral Re(I) complexes [14]. The average Re–N bond distance is 2.187 Å, larger than values previously reported for similar octahedral Re(I) complexes [6c, 15]. The bond angles between adjacent CO's are 86.1(2)–90.1(2)°, but the N(1)–Re–N(2) bite angle is 74.91(15)°. The dihedral angle between the two pyridyl rings is 7.3°, and the dihedral angle between the aromatic ring and the adjacent pyridyl ring is 69.0°.

Table 3. Photophysical, electrochemical, thermal, and IR data for **1** and **2**.

Complex	λ_{abs}[a] (nm) $\varepsilon \times 10^3$ $(mol\,L^{-1})^{-1}\,cm^{-1}$	λ_{em}[b] (nm)	λ_{ex}[c] (nm)	λ_{em}[d] (nm)	Lifetime (ns)	E^{ox}_{onset}[e] (v)	E^{red}_{onset}[e] (v)	E^{red}[f] (v)	Td[g] (°C)	IR (cm^{-1}) CO
1	283 (17.1) 363 (3.9)	574	356 430	550	13.48	0.99	–1.57	–1.52	299	1880, 1910, 2018
2	296 (16.8) 384 (3.1)	573	379 421	547	18.23	0.64 0.99	–1.56	–1.51	308	1870, 1922, 2024

[a]Maximum absorption wavelength, measured in CH_2Cl_2.
[b]Maximum emission wavelength, measured in CH_2Cl_2.
[c]Maximum excitation wavelength, measured in the solid state.
[d]Maximum emission wavelength, measured in the solid state.
[e]Estimated by CV using a platinum disc as the working electrode, platinum wire as auxiliary electrode, Ag/Ag^+ as reference electrode with ferrocene as the internal standard, Bu_4NBF_4 as supporting electrolyte in CH_3CN.
[f]These data were estimated according to the following formula: $\Delta E = 1240/\lambda^{abs}_{onset} = E^{ox}_{onset} - E^{red}$.
[g]Thermal decomposition temperature.

The dihedral angles in **1** are slightly different to the values for group 12 complexes with the same ligand [12].

Different supramolecular interactions, such as π–π stacking interactions, weak hydrogen-bonding, and CH$\cdots\pi$ interactions, play a very important role in construction of multi-dimensional supramolecular architectures. In **1**, the methoxy group donates a hydrogen bond to the carbonyl oxygen of an adjacent molecule with H$\cdots$O distance of 2.99(8) Å; the C–H$\cdots$O angle is 131(4)° (see table S1). Chloride bound to the metal center in an adjacent molecule interacts with hydrogen of the pyridyl in the next molecule, forming a weak hydrogen bond; the H$\cdots$Cl distance is 2.74(0) Å and the C–H$\cdots$Cl angle is 144(4)°. The two hydrogen bonds in **1** organize the metal complexes into 1-D chains parallel to the *a*-axis (figure S1). The chains are bound together into 2-D sheets in the *ac*-plane by weak CH$\cdots\pi$ and π–π stacking interactions between type A molecules in one chain and type B molecules in an adjacent chain (figure S1). The distances of the CH$\cdots\pi$ and π–π interactions are 3.24 Å and 3.63 Å, respectively.

3.3. *Physical properties*

The photophysical properties of **1** and **2** are listed in table 3. The absorption spectra in dilute CH_2Cl_2, shown in figure 3(a), display a strong absorption at 290 nm and a broad absorption at 380 nm. The absorption at high energy is primarily due to π–π* transition of the pyridine, and the lower energy absorption is typically from the spin-allowed metal (dπ) to ligand (π*) charge transfer (MLCT) [16]. Complexes **1** and **2** show similar emission bands and the emission peaks are 570 nm in CH_2Cl_2 solution. In the solid state, the emission maxima of complexes blue shift to 550 nm compared with their corresponding emission maxima in solution, and the emission bands are derived from the ^{3}MLCT exited state (figure 3b). The excited state lifetimes of complexes were determined by exponential decay curve-filling analysis in CH_2Cl_2 (table 3 and figure 4). The short excited state lifetime may provide the opportunity to use them for highly efficient OLEDs.

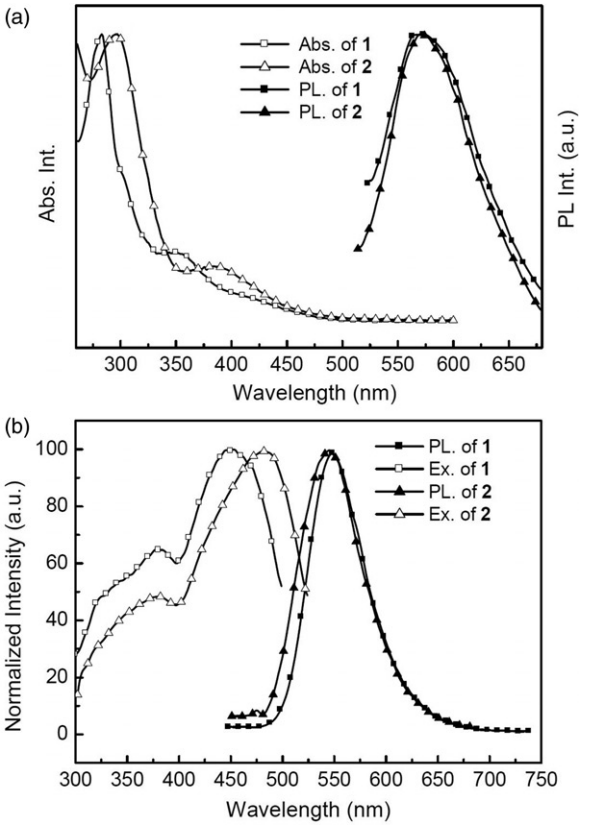

Figure 3. (a) Absorption and emission spectra of **1** and **2** in CH_2Cl_2; (b) the excitation and emission spectra of **1** and **2** in the solid state.

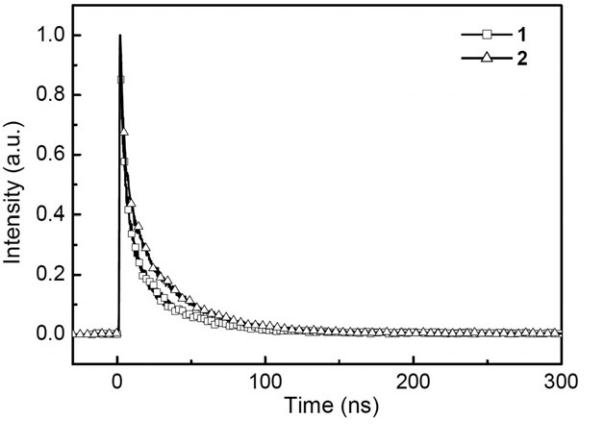

Figure 4. Photoluminescence lifetime decay measurements of **1** and **2** in CH_2Cl_2.

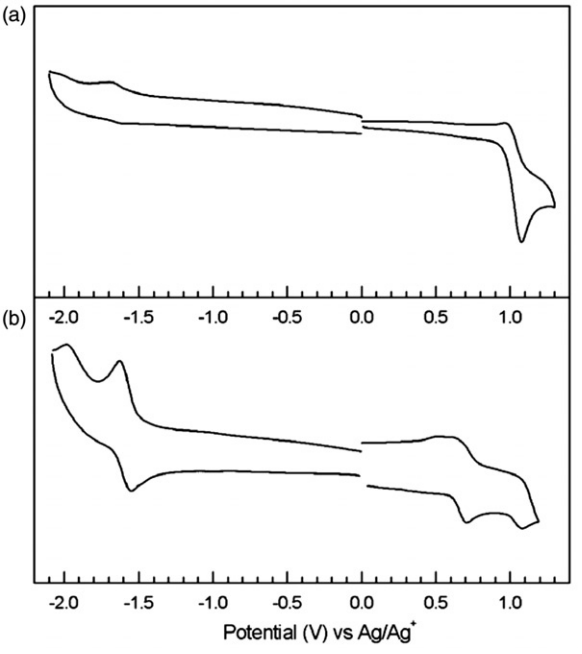

Figure 5. CV curves of **1** (a) and **2** (b) measured in CH_3CN at $0.1\,V\,s^{-1}$ scan rate.

TGA was performed to investigate their thermal stability. The complexes show high thermal decomposition temperatures (300°C and 308°C), which demonstrate their good thermal stability. The TGA traces exhibit two thermal decomposition processes (figure S2). In the first, **1** and **2** lose ~35% and ~50% weight, respectively, attributed to loss of the carbonyl and chloride and partial decomposition of the ligands, while the second weight loss is loss of their ligands. The good thermal stability of new rhenium(I) complexes is important for application in OLEDs.

Both complexes show a reduction reaction with reduction potential of −1.52 V to −1.51 V in CH_3CN, assigned to the redox couple of pyridine [17]. For **1**, an oxidation with potential about +0.99 V was observed, associated with the Re^{I}/Re^{II} redox couple. In contrast to **1**, two oxidation reactions were observed for **2**. The first oxidation at potential around +0.64 V could be ascribed to oxidation of the triphenylamine in its ligand [18], while the second oxidation reaction with potential about +0.99 V should be for the Re^{I}/Re^{II} redox couple (figure 5).

3.4. *EL properties*

Polymer-based, light-emitting diodes with **1** as a dopant were fabricated by spin casting and their EL performances were investigated. There are few reports on EL devices using solution processable rhenium(I) complexes as the emission layer and their EL performances are not predictable [9]. The solid state structural analysis of **1** showed that the discrete molecules interact strongly with each other *via* secondary interactions.

Table 4. Summary of the performance of OLEDs based on **1**.

Concentration (wt%)	η_1 [a] (cd A^{-1})	η_2 [b] (cd A^{-1})	B_{max} [c] (cd m^{-2})	η_3 [d] (lm W^{-1})
0.5	2.38	1.66	3050	1.18
1.0	2.97	2.40	2392	1.29
2.0	2.33	1.91	2228	1.03

[a]Maximum efficiency.
[b]Efficiency at 1000 cd m^{-2}.
[c]Maximum brightness.
[d]Maximum power efficiency.

However, if these molecules become dispersed when **1** is incorporated in a polymer host, then the performance of the device will be increased. The polymer blend PVK–PBD (40%) was selected as the host, which emission band overlaps the absorption bands of **1**. PVK is a good hole-transporting material while PBD is an electron-transporting material. Employment of the PVK–PBD mixture host would enhance balance of carriers in light-emitting layer and thus enhance the emitting efficiency of devices [19]. Indium-tin-oxide (ITO) glass and aluminum were used as the anode and cathode, respectively. Poly(3,4-ethylenedioxythiophene) : poly(styrene sulfonate) (PEDOT : PSS) and LiF were used as materials for facilitating the hole and electron injection from the two electrodes, and 2,2′,2″-(1,3,5-benzenetriyl)tris[1-phenyl-benzimidazole] (TPBI) was chosen as an electron-transporting material. The structure of the devices is as follows: ITO/PEDOT : PSS (40 nm)/PVK : PBD (40 wt%): *X* wt% **1** (80 nm)/TPBI (40 nm)/LiF (0.7 nm)/Al (100 nm)(X = 0.25, 1.0, 2.0). Complex **1** was doped into the host PVK–PBD at 0.25–2.0 wt% as the light-emitting layer. The thickness of the doped light-emitting layer is about 80 nm. The TPBI layer and the electrode layers were deposited by a resistive heating method.

The performance parameters of OLEDs based on 0.25, 1.0 and 2.0 wt% **1** in PVK–PBD blends of the devices are listed in table 4. The 1.0 wt% doping concentration is most suitable for obtaining high EL efficiency. The current density (J) and luminance (L) *versus* applied voltage (V) characteristics of the device based on **1** with different doping concentration are shown in figure 6(a). For the 1.0 wt% of **1** doped device, the turn-on voltage is 6.8 V (at brightness of 1 cd m^{-2}). This device has a luminance of 720 cd m^{-2} at 10 V and current density of 38.46 mA cm^{-2}, and the luminance reaches near 3050 cd m^{-2} at 13 V and current density of 230.57 mA cm^{-2}. The value of maximum brightness observed for the EL device based on **1** are higher than the 960 cd m^{-2} previously reported for a device based on [$Re_2(\mu\text{-}Cl)_2(CO)_6(\mu\text{-diazine})$] incorporated into PVK polymer with a device structure of ITO/PEDOT : PSS/PVK:$Re_2(\mu\text{-}Cl)_2(CO)_6(\mu\text{-diazine})$/TPBI/Ba/Al [9b] and higher than 730 cd m^{-2} for a rhenium(I) complex with 2,2′-bipyridine doped in host material of polycarbonate (PC) and the device configuration of ITO/PVK : Re: PC/Al [9c]. Figure 6(b) shows the luminous efficiency (LE) as a function of the current density (J) of the device made from PVK–PBD with 0.25, 1.0, and 2.0 wt% **1**. Efficiencies of the devices increase as the current densities increase at first and decrease after reaching the maximum value. The LE_{max} is from 2.38, 2.97, and 2.33 cd A^{-1} for 0.25–2% doping concentration of **1**, respectively. For larger doping concentration (>3%) the device efficiency decreases significantly (not shown here). The value of maximum current efficiency observed for the EL devices studied in this article exhibit little enhancement with respect to [$Re_2(\mu\text{-}Cl)_2(CO)_6(\mu\text{-1,2-diazine})$], which the best previously reported

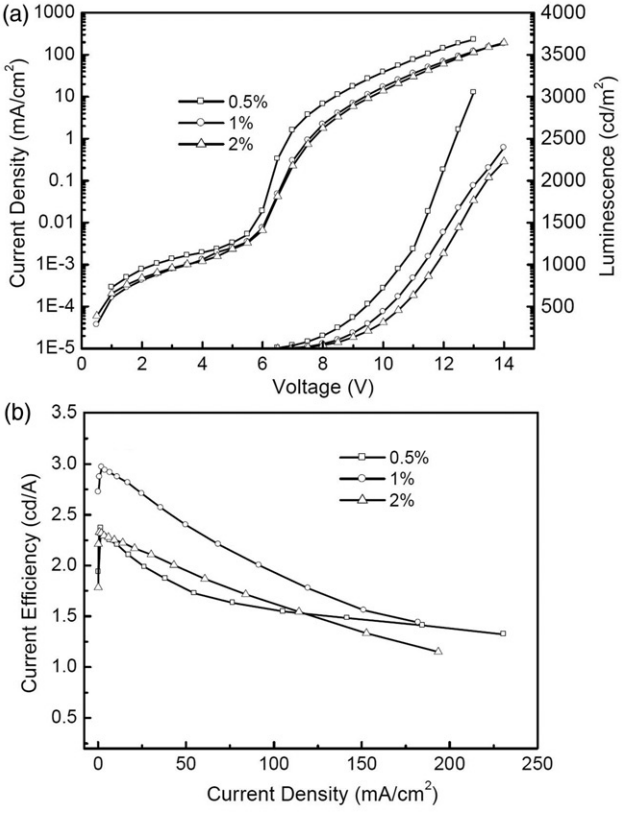

Figure 6. (a) Current density–brightness–voltage curves and (b) current efficiency–current density curves of devices based on **1** with different concentrations.

value (2.1 cd A^{-1}) [9d]. When the luminance reaches to 1000 cd m^{-2}, the 1.0 wt% of **1** doped device still exhibits a maximum current efficiency of 2.4 cd A^{-1}. The slow decrease in current efficiency with increasing current density has been attributed to saturation of the phosphorescence sites under these conditions not being severe due to the short triplet lifetime of the light-emitting material [5b]. Nevertheless, the performances of these devices are greatly improved in comparison with the previously reported results from OLEDs fabricated by solution processable rhenium(I) complexes [8].

4. Conclusion

Two new rhenium(I) complexes with substituted 2,2′-bipyridine ligands have been synthesized. Crystal structure analysis revealed that the coordination geometry of rhenium can be described as distorted octahedral defined by one chloride, facial arrangement of three carbonyls, and the diimine. The rhenium(I) complexes exhibit bright yellow luminescence with relatively short triplet lifetime in solution. High-efficiency, polymer-based electrophosphorescent light-emitting devices have been

fabricated using **1** as dopant and PVK–PBD as host. The device exhibits a maximum current efficiency of 2.97 cd A^{-1} and peak brightness in excess of 2390 cd m^{-2}. These performances are best reported for devices by spin-casting technology employing solution rhenium(I) complex as emission layer.

Supplementary material

CCDC 841690 contains the supplementary crystallographic data for **1**. These data can be obtained free of charge at http://www.ccdc.cam.ac.uk (or from the Cambridge Crystallographic Data Centre, 12 Union Road, Cambridge CB2 1EZ, UK; Fax: +44-1223-336-033; E-mail: deposit@ccdc.cam.ac.uk).

Acknowledgments

This work was supported by the National Natural Science Foundation of China (Nos 21074043 and 60978062).

References

[1] M.A. Baldo, D.F. O'Brian, Y. You, A. Shoustikov, S. Sibley, M.E. Thompson, S.R. Forrest. *Nature*, **395**, 151 (1998).
[2] (a) H. Sasabe, J. Takamatsu, T. Motoyama, S. Watanabe, G. Wagenblast, N. Langer, O. Molt, E. Fuchs, C. Lennartz, J. Kido. *Adv. Mater.*, **22**, 5003 (2010); (b) M. Bandini, M. Bianchi, G. Valenti, F. Piccinelli, F. Paolucci, M. Monari, A. Umani-Ronchi, M. Marcaccio. *Inorg. Chem.*, **49**, 1439 (2010).
[3] Y. Unger, D. Meyer, O. Molt, C. Schildknecht, I. Munster, G. Wagenblast, T. Strassner. *Angew. Chem. Int. Ed.*, **49**, 10214 (2010).
[4] (a) H. Xia, Y.Y. Zhu, D. Lu, M. Li, C.B. Zhang, B. Yang, Y.G. Ma. *J. Phys. Chem. B*, **110**, 17784 (2006); (b) H. Xia, M. Li, D. Lu, C.B. Zhang, W.J. Xie, X.D. Liu, B. Yang, Y.G. Ma. *Adv. Funct. Mater.*, **17**, 1757 (2007); (c) H. Xia, C.B. Zhang, S. Qiu, P. Lu, J.Y. Zhang, Y.G. Ma. *Appl. Phys. Lett.*, **84**, 290 (2004).
[5] (a) F. Li, M. Zhang, G. Cheng, J. Feng, Y. Zhao, Y.G. Ma, S.Y. Liu, J.C. Shen. *Appl. Phys. Lett.*, **84**, 148 (2004); (b) G. Che, Z. Su, W. Li, B. Chu, M. Li, Z. Hu, Z. Zhang. *Appl. Phys. Lett.*, **89**, 103511 (2006).
[6] (a) C.B. Liu, J. Li, B. Li, Z.R. Hong, F.F. Zhao, S.Y. Liu, W.L. Li. *Appl. Phys. Lett.*, **89**, 243511 (2006); (b) X. Li, D.Y. Zhang, W.L. Li, B. Chu, L.L. Han, J.Z. Zhu, Z.S. Su, D.F. Bi, D. Wang, D.F. Yang, Y.R. Chen. *Appl. Phys. Lett.*, **92**, 083302 (2008); (c) Z.J. Si, J. Li, B. Li, F.F. Zhao, S.Y. Liu, W.L. Li. *Inorg. Chem.*, **46**, 6155 (2007).
[7] A.J. Lees. *Coord. Chem. Rev.*, **177**, 3 (1998).
[8] (a) M.V. Werrett, D. Chartrand, J.D. Gale, G.S. Hanan, J.G. Maclellan, M. Massi, S. Muzzioli, P. Raiteri, B.W. Skelton, M. Silberstein, S. Stagni. *Inorg. Chem.*, **50**, 1229 (2011); (b) J.M. Villegas, S.R. Stoyanov, W. Huang, D.P. Rillema. *Dalton Trans.*, 1042 (2005); (c) R. Horvath, C.A. Otter, K.C. Gordon, A.M. Brodie, E.W. Ainscough. *Inorg. Chem.*, **49**, 4073 (2010); (d) M.G. Fraser, A.G. Blackman, G.I.S. Irwin, C.P. Easton, K.C. Gordon. *Inorg. Chem.*, **49**, 5180 (2010).
[9] (a) Y.Y. Lu, C.C. Ju, D. Guo, Z.B. Deng, K.Z. Wang. *J. Phys. Chem. C*, **111**, 5211 (2007); (b) M. Mauro, E.Q. Procopio, Y.H. Sun, C.H. Chien, D. Donghi, M. Panigati, P. Mercandelli, P. Mussini, G. D'Alfonso, L. De Cola. *Adv. Funct. Mater.*, **19**, 2607 (2009); (c) W.K. Chan, P.K. Ng, X. Gong, S.J. Hou. *Appl. Phys. Lett.*, **75**, 3920 (1999); (d) Y.P. Wang, W.F. Xie, B. Li, W.L. Li. *Chin. Phys. Lett.*, **18**, 1501 (2007); (e) G. David, P.J. Walsh, K.C. Gordon. *Chem. Phys. Lett.*, **383**, 292 (2004).
[10] *SHELXTL*, PC Siemens Analytical X-ray Instruments, Madison, WI (1993).

[11] G.M. Sheldrick. *SHELXTL Structure Determination Programs (Version 5.0)*, PC Siemens Analytical Systems, Madison, WI (1994).
[12] X.M. Liu, X.Y. Mu, H. Xia, L. Ye, W. Gao, H.Y. Wang, Y. Mu. *Eur. J. Inorg. Chem.*, 4317 (2006).
[13] M. Zhang, P. Lu, X.M. Wang, H. Xia, W. Zhang, B. Yang, L.L. Liu, L. Yang, M. Yang, Y.G. Ma, J.K. Feng, D.J. Wang. *Thin Solid Films*, **477**, 193 (2005).
[14] (a) D.L. Reger, R.P. Watson, M.D. Smith, P.J. Pellechia. *Organometallics*, **25**, 743 (2006); (b) D.L. Reger, R.P. Watson, M.D. Smith. *J. Organomet. Chem.*, **692**, 3094 (2007); (c) A. Brink, H.G. Visser, A. Roodt. *J. Coord. Chem.*, **64**, 122 (2011).
[15] (a) Q.H. Wei, G.Q. Yin, L.Y. Zhang, Z.N. Chen. *Inorg. Chem.*, **45**, 10371 (2006); (b) F. Kennedy, N.M. Shavaleev, T. Koullourou, Z.R. Bell, J.C. Jeffery, S. Faulkner, M.D. Ward. *Dalton Trans.*, 1492 (2007); (c) S. Dehghanpour, J. Lipkowski, A. Mahmoudi, M. Khalaj. *J. Coord. Chem.*, **63**, 1473 (2010).
[16] K.K.W. Lo, J.S.Y. Lau, V.W.Y. Fong, N.Y. Zhu. *Organometallics*, **23**, 1098 (2004).
[17] C.V. Krishnan, C. Creutz, H.A. Schwarz, N. Sutin. *J. Am. Chem. Soc.*, **105**, 5617 (1983).
[18] Z.H. Li, M.S. Wong, H. Fukutani, Y. Tao. *Org. Lett.*, **8**, 4247 (2006).
[19] X. Gong, M.R. Robinson, J.C. Qstrowski, D. Moses, G.C. Bazan, A.J. Heeger. *Adv. Mater.*, **14**, 581 (2002).